PHOTONICS Research

Intelligent reconfigurable metasurface for self-adaptively electromagnetic functionality switching

Ying She,[1,2,3] Chen Ji,[1] Cheng Huang,[1,3] Zuojun Zhang,[1] Jianming Liao,[1,3] Jiangyu Wang,[1,2,3] and Xiangang Luo[1,3,*]

[1]State Key Laboratory of Optical Technologies on Nano-Fabrication and Micro-Engineering, Institute of Optics and Electronics, Chinese Academy of Sciences, Chengdu 610209, China
[2]School of Optoelectronic Science and Engineering, University of Electronic Science and Technology of China, Chengdu 610054, China
[3]School of Optoelectronics, University of Chinese Academy of Sciences, Beijing 100049, China
*Corresponding author: lxg@ioe.ac.cn

Received 3 December 2021; revised 26 January 2022; accepted 26 January 2022; posted 28 January 2022 (Doc. ID 450297); published 1 March 2022

Reconfigurable metasurfaces have attracted a deal of attention owing to their multifunctional and dynamic electromagnetic (EM) manipulation properties. However, most of the previous reconfigurable metasurfaces rely on manual control for function switching, which has huge limitations in practical application. Here, an intelligent metasurface with the self-adaptively EM manipulation capability is proposed. It integrates the sensing-and-feedback components to construct a closed-loop system, which can automatically adjust EM functionalities for the different incident power information. The sensing module in this metasurface can first perceive the incident EM power intensity and then provide the feedback signal to the field programmable gate array controlling platform that can send the corresponding instruction to the executing material for switching the EM functionality among transmission, reflection, and tunable absorption. Good self-adaptive reaction capability and practicability of the proposed metasurface have been demonstrated by the experiment. It has the capability of making a real-time response with adaptive EM behavior to the varying incoming wave power without the aid of human beings. Our design provides an avenue toward intelligent and cognitive metasurfaces, which has extensive application prospects in smart skin, intelligent absorber, and the related EM fields.

https://doi.org/10.1364/PRJ.450297

1. INTRODUCTION

During the past few decades, intelligent electromagnetic (EM) materials have attracted great attention owing to their tremendous application prospects, such as adaptive camouflage, intelligent cloaking, and smart skin [1]. Although there is no generally acknowledged definition of intelligent EM material, it can be understood as the ability to perceive external information and to make a feedback response with adaptive EM behavior to a changing environment [2]. A basic form of intelligent EM material can be defined on the material level by integrating various functional elements, including sensor, actuator, and memory [3]. Herein, the design of the material is very important, which is required to have the capability of handling multitasking for adapting their EM functionalities to the different environments. Recently, the emerging reconfigurable metasurface provides a good research platform for material design, because it can integrate various EM functionalities into itself, and these functionalities can be rapidly and dynamically switched with the external stimuli [4–8]. Therefore, the reconfigurable metasurface could be considered as a desirable candidate to construct intelligent EM material.

There have been various control mechanisms explored for the design of reconfigurable metasurface to achieve dynamic modulation of EM waves, such as thermal effect [9], electrical tuning [10], optical illumination [11], mechanical stretching [12], and micro-electro-mechanical systems (MEMS) [13]. Two typical structural forms have been developed to construct reconfigurable metasurfaces. One approach is to combine the passive metastructure with tunable materials, including phase change materials [14,15], two-dimensional (2D) materials (i.e., graphene and MoS_2) [16–18], and liquid crystals [19], for realizing active function switching. The other one is to integrate positive–intrinsic–negative (PIN) diodes, or varactors into the design of metastructures, which is generally adopted by most of the existing reconfigurable metasurfaces at microwave frequencies [20–32]. One can dynamically control EM responses by tuning external bias voltages to the above

lumped components. Many works have employed the PIN diodes to design 1-bit or multi-bit coding metasurfaces for wavefront manipulation [21–25]. In contrast to discrete phase modulation with PIN diodes, the continuous phase control can be realized by introducing varactors instead [26–28]. In addition, the PIN diode can be also used for constructing tunable absorbers by modulating its forward resistances [29,30]. Based on appropriate structure design with lumped components, reconfigurable metasurfaces can be established with multifunctional EM properties. In Ref. [31], a reconfigurable metasurface integrated with PIN diodes and varactors was proposed to simultaneously realize three different EM functionalities which are beam steering, polarization transformation, and backscattering reduction, respectively. In Ref. [32], the reported metasurface can be freely switched from transmission to reflection and then perfect absorption in real time. However, the abovementioned EM switching must rely on the control by human beings.

In order to achieve intelligent manipulation of EM waves without human intervention, reconfigurable metasurfaces should be further equipped with a sensor, actuator, and memory unit, which could rapidly and self-adaptively adjust its EM functionalities within the varying environment, just like a chameleon. Similar schemes have been proposed to design smart metasurfaces [33–35]. In the latest research [33], the smart metasurface integrated with a power detector was proposed to adaptively modulate the reflected patterns under the different microwave incidences. In Ref. [35], the intelligent cloak combining detectors and the deep-learning algorithm was reported, which can realize adaptive camouflage in response to the ever-changing incident wave and background through real-time phase compensation.

Here, an intelligent metasurface with the capability of self-adaptively EM manipulation is proposed. Compared with the traditional reconfigurable metasurface, it further integrates the sensing-and-feedback components to construct a closed-loop system without the aid of human beings. Our intelligent metasurface can first sense the incident EM power intensity, then acquire an operation instruction from the field programmable gate array (FPGA) controlling platform, and finally make dynamic switching of its EM functionality among reflection, transmission, and tunable absorption. Each of the EM functionalities depends on the power intensity of the incident EM wave. We have experimentally demonstrated that the proposed intelligent metasurface can not only realize high transmission for communication but also be switched to perform the strong absorption performance for reducing the probability of being detected by the threat radar. In addition, it can also behave the reflection property for avoiding EM interference. More importantly, the above EM functionalities are adaptively switched, which depends on the power intensity of the incident wave. Such design may inspire some potential applications in smart skin, radar radome, and the related EM fields.

2. DESIGN AND METHODS

A. Principle of the Intelligent Metasurface

Figure 1 shows the schematic configuration of the proposed intelligent metasurface, which consists of three main parts: power detecting module, FPGA controlling platform, and the executing material. The power detecting module serves as a

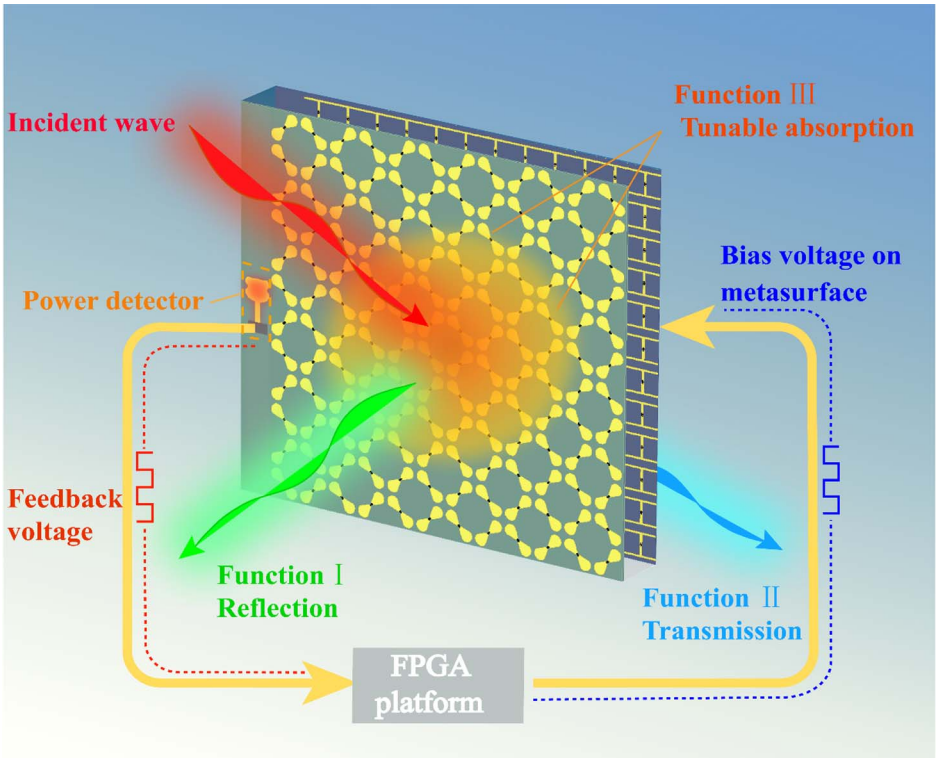

Fig. 1. Schematic configuration of the proposed intelligent metasurface.

sensor to perceive the intensity of the illuminating wave and then transforms the microwave signal into the feedback voltage for the FPGA controlling platform. The FPGA platform is mainly used for information processing, which can analyze the feedback voltage from the power detecting module and then send the proper instruction to the executing material for automatically adjusting its EM property with response to the changes of the EM environment. Many voltage configurations need to be pre-stored in the FPGA platform for controlling the operation state of the proposed executing material. Here, the executing material adopts the metasurface form that can generate three different EM functionalities including reflection, transmission, and tunable absorption by applying the corresponding voltage configuration to the loaded PIN diodes. When the power intensity of the incident EM wave is very low, the executing metasurface exhibits the high reflection property. If the power intensity is increased to a threshold value, it will be switched to the transmission function, which can realize communication with the outside. However, when the illuminating EM power intensity is continuously enhanced, the operation state of the proposed metasurface would be automatically changed to the absorption mode because the incoming wave may originate from threat radar in this case. In addition, the absorption performance would be gradually enhanced with the increase of the incidence intensity. All the above EM functionalities can be self-adaptively adjusted in the whole operation flow.

B. Design of the Reconfigured Metasurface

Figure 2(a) shows the geometrical model of the unit cell for the proposed executing metasurface, which is composed of two-layer functional structures separated by a foam spacer. The bottom-layer functional structure is made of two layers of T-type metallic patches, which are orthogonally arranged on both sides of a 0.508 mm thick F4B ($\varepsilon_r = 2.65$ and loss tangent of 0.007) dielectric substrate. A pair of PIN diodes 1 are respectively loaded between the two T-type patches on the upper and bottom metallic layers. The transmission/reflection

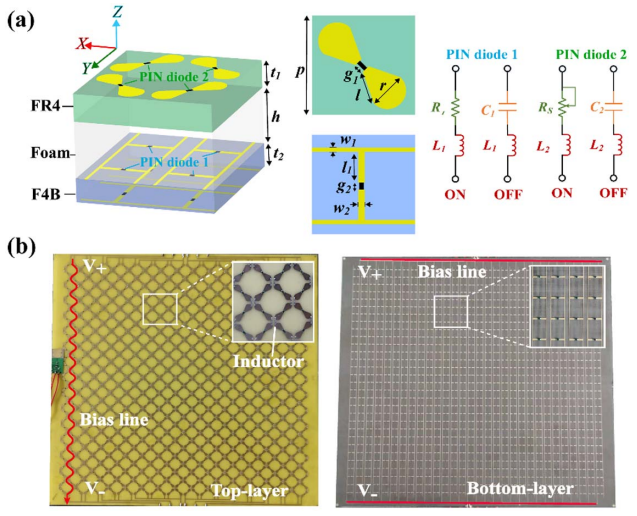

Fig. 2. (a) Geometrical model of the unit cell for the executing metasurface. (b) Photography of the fabricated metasurface sample. The metallic patterns on the top layer are serially connected in each row, while they are connected in parallel on the bottom layer.

characteristics of the bottom-layer structure can be analyzed by using LC resonant circuit, and the dynamic switching of PIN diode 1 would make the whole structure generate the bandpass or bandstop state [36]. The top-layer functional structure consists of four symmetric bowtie-shaped patches etched on the FR4 dielectric substrate ($\varepsilon_r = 4.4$ and loss tangent of 0.02) with thickness of 0.8 mm. PIN diode 2 is embedded between adjacent bowtie-shaped patches, and its resistance can be tuned through the change of the forward current. When the bottom-layer structure operates at the reflection mode, the whole metasurface could exhibit good absorbing performance at a specific resistance of PIN diode 2 where its input impedance would be well matched with the free space impedance based on the transmission-line theory. If the diode resistance deviates from the ideal value, the reflection amplitude would be deteriorated due to the mismatch between the input impedance and the free space impedance. So we can further dynamically control the reflection amplitude of this metasurface by tuning the resistance of PIN diode 2. In addition, the entire metallic structures on both layers behave relatively in geometrical symmetry, making the executing metasurface possess a polarization-insensitive property [7].

The geometrical parameters of the proposed metasurface are optimized as follows: $p = 12$ mm, $l = 4$ mm, $r = 4.5$ mm, $g_1 = 0.8$ mm, $g_2 = 1$ mm, $l_1 = 4$ mm, $w_1 = 0.15$ mm, $w_2 = 0.6$ mm, $t_1 = 0.8$ mm, $h = 6.5$ mm, and $t_2 = 0.508$ mm. PIN diode 1 of SMP1321-079LF manufactured by Skyworks was selected as a switch in our design. In the simulation, it can be considered as high capacitance ($C_1 = 0.3$ pF) in the OFF state and small resistance ($R_1 = 2\ \Omega$) in the ON state. Its package structure would introduce a series inductance of $L_1 = 0.7$ nH. The model of BAP70-02 from NXP Semiconductors is chosen for PIN diode 2, whose resistance of R_s can be changed between 2 and 80 Ω. The diode capacitance and series inductance are $C_2 = 0.57$ pF and $L_2 = 0.6$ nH, respectively. Figure 2(b) shows the photography of the fabricated metasurface sample, which is composed of 30 × 30 unit cells fabricated by printing circuit technology. In the biasing network of the top layer, three series-connected inductors with values of 3.2, 6.8, and 10 nH (from TY-COMPAS) were inserted between the bowtie-shaped patches of the neighboring unit cells, which can effectively isolate the wideband RF signal.

In order to demonstrate the tunable EM manipulation function of the proposed executing metasurface, the numerical simulation is conducted by the commercial software of CST Microwave Studio. The period boundary condition is set to the four sides of the unit cell for evaluating the infinite array. The Floquet port is defined as the exciting port to generate the plane wave normally incident onto the unit cell. Table 1 lists the operation states of the two kinds of PIN diodes corresponding to the three different EM functionalities of our metasurface. For the reflection mode, it is seen in Fig. 3(a) that high reflection property is obtained in the frequency range from 5 to 10 GHz when PIN diodes 1 and 2 respectively operate at the ON and OFF states. The measured average reflection loss is about 1 dB, indicating 79.4% reflectivity. If all the PIN diodes are switched off, the metasurface would be changed to the transmission mode where the insertion loss is less than 1.5 dB between 5 and 5.25 GHz as shown in Fig. 3(b). When PIN

Table 1. PIN Diode Configurations for the Different EM Functionalities of the Proposed Metasurface

Function	State of PIN Diode 1	State of PIN Diode 2
Reflection	ON	OFF
Transmission	OFF	OFF
Tunable absorption	ON	Tunable resistance
	ON	
	ON	

diodes 1 are switched on and the resistance of PIN diodes 2 is set as 80 Ω, it is obvious that there is almost no reflection and transmission at the frequency band of 4.8–10 GHz. As Figs. 3(c) and 3(d) show, both the reflection and transmission coefficients are lower than −10 dB, which means that our metasurface realizes broadband absorption performance in this case. In addition, if the resistance of PIN diodes 2 is further varied from 80 to 10 Ω, the transmission property has no obvious variation, but the reflection amplitude realizes about 15 dB tuning range as seen in Fig. 3(d). This result indicates that our metasurface can realize dynamic absorption with different reflection amplitude. The measured results agree well with the simulated ones, although there is still a little frequency deviation between them, which may be due to the fabrication tolerance and the slight difference between the simulation condition and measurement environment.

C. Design of the Sensing Module

To realize the self-adaptive response to the changes of environmental EM wave, the sensing module is designed as a power detector for perceiving the incident power intensity, which is directly integrated into the left side of the top-layer structure of the proposed executing metasurface. As Fig. 4(a) shows, the power detector is composed of an ultra-wideband (UWB) patch antenna and a power detecting chip (LTC5530 of Linear Technology) with its peripheral circuit. The UWB antenna is made of an elliptical-shaped patch and a defected ground, which can realize miniaturization and wideband impedance matching. It is seen in Fig. 4(b) that the antenna gain curve is relatively flat, and the gain varying range is lower than 1.5 dB at the frequency band of 5–10 GHz. In addition, the designed antenna keeps almost the same radiation patterns at different frequencies, which can effectively reduce the probability of power detecting error. The patch antenna perceives the incident EM wave power and then transmits it to an RF power detector of LTC5530 that can rectify the EM signals into the different feedback voltages. Figure 4(c) shows the measured feedback voltages corresponding to the different illuminating power intensities. When the illuminating power intensity varies from −20 to 10 dBm, the feedback DC voltage of the LTC5530 is changed from 0.83 to 5.7 V, which will be injected into the FPGA platform.

D. Design of the FPGA Controlling Platform

The FPGA controlling platform is designed for processing information and generating the proper instruction for the executing metasurface. It is mainly composed of an FPGA chip and analog-digital-analog (ADA) modules. The selected FPGA chip is XC6SLX9 from ALINX Electronics Technology, and each ADA module contains an analog-to-digital converter (ADC) submodule and a digital-to-analog converter (DAC) submodule. The AD conversion chip of the ADC submodule is AD7476 from Analog Devices, which can provide a digital output signal of 0–4095 corresponding to the input voltage of

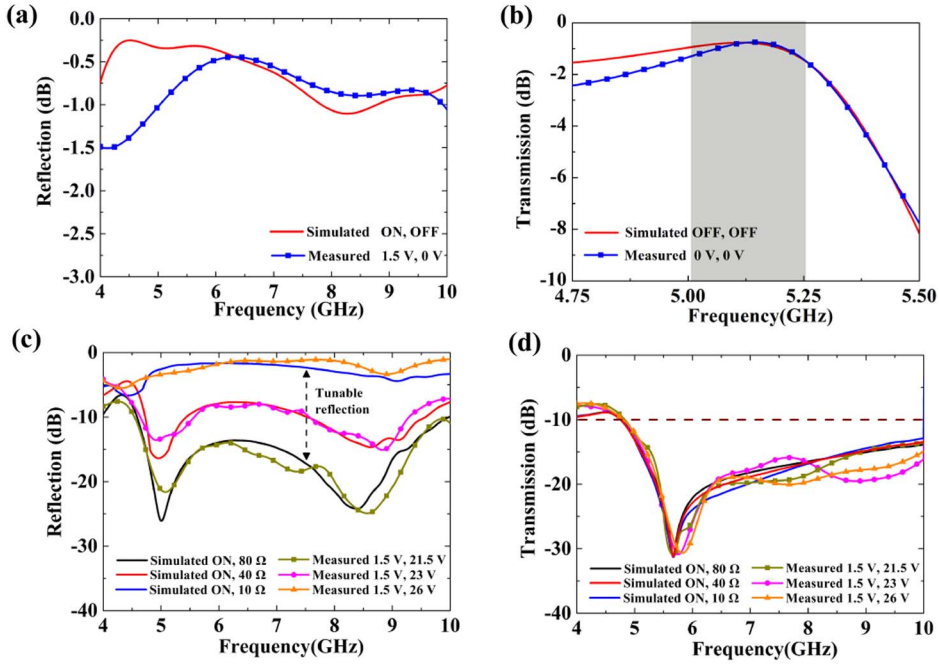

Fig. 3. Simulated and measured reflection/transmission properties of the proposed executing metasurface under the different operation modes with the corresponding diode configurations of (PIN diode 1, PIN diode 2). (a) Reflection mode. (b) Transmission mode. (c), (d) Reflection and transmission properties at the tunable absorption mode.

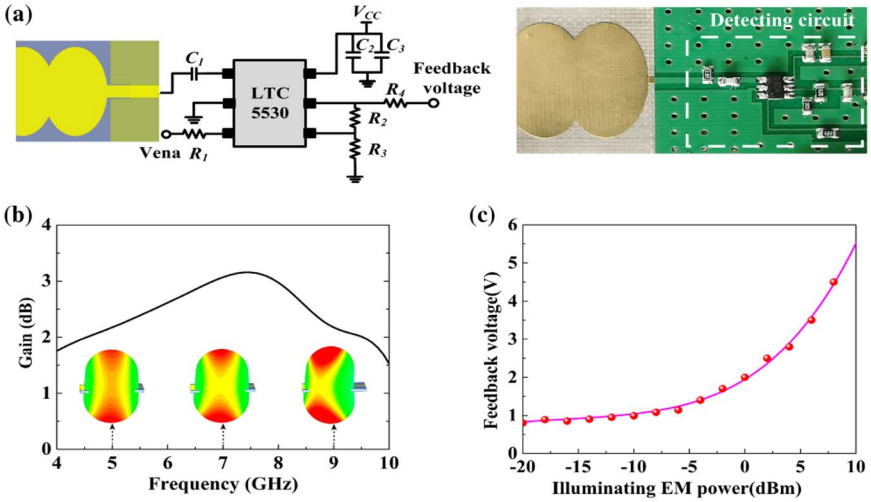

Fig. 4. (a) Configuration of the sensing module for the incident power detecting. It is composed of an ultra-wideband patch antenna and a power detecting chip with the peripheral circuit. Values of the circuit parameters are chosen as follows: $R_1 = 68$ kΩ, $R_2 = 82$ kΩ, $R_3 = 10$ kΩ, $R_4 = 10$ kΩ, $C_1 = 39$ pF, $C_2 = 100$ pF, $C_3 = 0.1$ μF. (b) Gain of the designed patch antenna and its radiation patterns at 5, 7, and 9 GHz. (c) Measured feedback voltage of the power detectors at 6 GHz for the different incident power intensities.

Table 2. Mapping Relationship among the Incident Power Intensity, Received Feedback Voltage, and Controlling Bias Voltage for the Different Layers of the Proposed Metasurface

Function	Illuminating Power (dBm)	Feedback Voltage (V)	Bias Voltage on Top-Layer Metasurface (V)	Bias Voltage on Bottom-Layer Metasurface (V)
Reflection	≤ −20	≤0.8	0	1.5
Transmission	−20 to −13	0.8–1	0	0
Tunable absorption	−13 to −9	1–1.4	24–27	1.5
	−9 to −2	1.4–2.2	22–24	1.5
	−2 to 10	≥2.2	19–22	1.5

0–12 V. Considering the received feedback voltage ranging from 0.83 to 5.7 V, the output digital signal of the ADC module would be located between 283 and 1946. The DAC submodule is equipped with a conversion chip of AD5621, which can provide the analog DC voltage of −6 to 9 V for our metasurface. In the design of the proposed metasurface, all PIN diodes 1 are in the parallel connection, while PIN diodes 2 are connected in series. So we applied the constant source voltage of 0 V and 25 V to the cathode of PIN diodes 1 and 2, respectively. Therefore, the bias voltage across PIN diodes 1 can be controlled between −6 and 9 V, while it is from 16 to 31 V for PIN diodes 2. The mapping relationship among the incident power intensity, the received feedback voltage, and the controlling bias voltage has been given in Table 2. The threshold for each case can be dynamically set at will according to the practical application environment.

3. EXPERIMENTAL MEASUREMENT AND DISCUSSION

To experimentally demonstrate the self-adaptive EM manipulation capability of the proposed intelligent metasurface, a measurement system as shown in Fig. 5 was set up in a microwave anechoic chamber. We utilized a vector network analyzer (VNA) and a power amplifier to generate an RF input signal with the adjustable power intensity for simulating the varying EM environment. The transmitted RF signal is captured by a spectrum analyzer through a low noise amplifier, while the reflected RF signal is received by another horn connected to the receiving port of the same VNA. With the variation of the illuminating power, our sample should automatically switch its EM functionalities.

Figure 6 shows the transmitted power intensity and reflection of the metasurface under the different power illuminations. For the transmission measurement, the setup was normalized without a sample, and the illumination power at the position of the sample bracket is fixed as −15 dBm at the different frequency points. For the reflection measurement, a metallic plate with an identical dimension was used as a reference to standardize the reflection coefficient. When the illuminating power is set as −20 dBm, the FPGA platform first receives the feedback information from the sensor and then chooses to send the voltage configuration of the reflection mode to the sample. As Figs. 6(a)–6(g) show, the transmitted signal received by the spectrum analyzer is very weak, while the corresponding reflection is as high as about −1 dB as seen in Fig. 6(h). That means our sample behaves the high reflection property in this case. If the illuminating power is increased to −15 dBm, the transmitted signal is still weak at most of the frequency points except for 5 and 5.2 GHz, where the transmission loss is only about −1.4 and −0.8 dB, respectively.

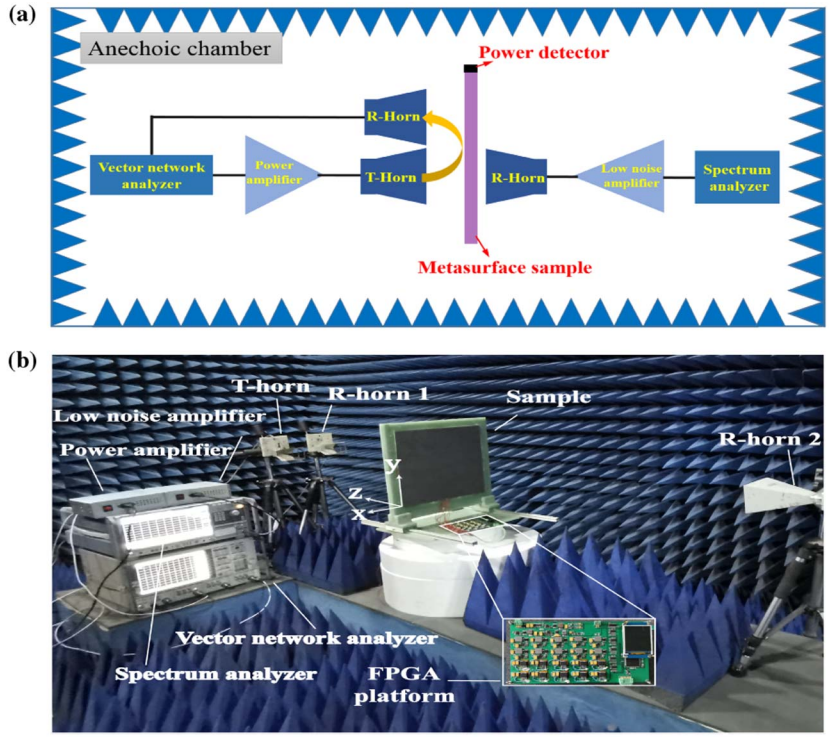

Fig. 5. (a) Sketch of the measurement system for the intelligent metasurface and (b) photograph of the measurement setup in the microwave anechoic chamber.

Therefore, the narrowband transmission performance is realized by our sample. As the incident power is further enhanced, the captured transmission signal intensity seems to be also gradually increased compared with the case of −20 dBm power illumination. However, considering the increment of the incident power, the calculated transmittance of our sample is very low and less than −10 dB at all frequency points as displayed in Fig. 6(i). For the reflection property of the sample under the illumination with the large power intensity, it is obvious in Fig. 6(h) that the average reflectivity can be dynamically tuned from −2.5 to −22.8 dB as the illuminating power is increased from −11 to 0 dBm, indicating that our sample can exhibit more and more powerful absorption performance with the increase of incidence power. The above results have fully demonstrated that the proposed intelligent metasurface has the capability of self-adaptively achieving functionality switching among transmission, reflection, and tunable absorption for the different incidence power intensities. In addition, it should be pointed out that although the executing metasurface has the polarization insensitivity property [7], the intelligent metasurface can just work under the single polarization mode, which is mainly limited by the design of the single-polarized detecting unit. If achieving dual-polarized operation, one can simultaneously employ the two UWB patch antennas placed in the orthogonal distribution or just design the dual-polarized patch antenna instead.

4. CONCLUSION

In summary, we have proposed an intelligent metasurface that can achieve self-adaptive EM manipulation with response to the different incident EM information. It is mainly composed of three parts: the sensing module, the FPGA controlling platform, and the executing material. The sensing module can perceive the power intensity of the incident EM wave, while the FPGA platform is used for information processing and thus sends the instruction to the executing material for switching its EM functionality among transmission, reflection, and tunable absorption. The whole metasurface establishes the complete sensing-feedback system, and its operation flow is automatic without human intervention. We have experimentally demonstrated the self-adaptive EM manipulation capability of our sample, which can make real-time and automatic adjustment of its operation state according to the perceived power intensity of the incoming wave. Compared with the traditional reconfigurable metasurface, our design further promotes the development of metasurfaces from manual control to self-adaptive control, which may find potential application in intelligent materials and systems.

5. EXPERIMENTAL SECTION

As shown in Fig. 5(b), the experimental setup was established in a microwave anechoic chamber. A VNA (R&S ZVA40) was adopted as the signal source and receiver for reflection measurement. Its port 1 was connected to a power amplifier with a gain of 20 dBi, and the amplified signal was transmitted through an LP standard horn (T-horn). The reflected signal was received by R-horn 1 connected to the other port of the VNA, while the transmitted signal would be captured by R-horn 2 and then transferred to the spectrum analyzer (R&S FSW50) through an LNA (with a gain of 15 dB). The distance between the

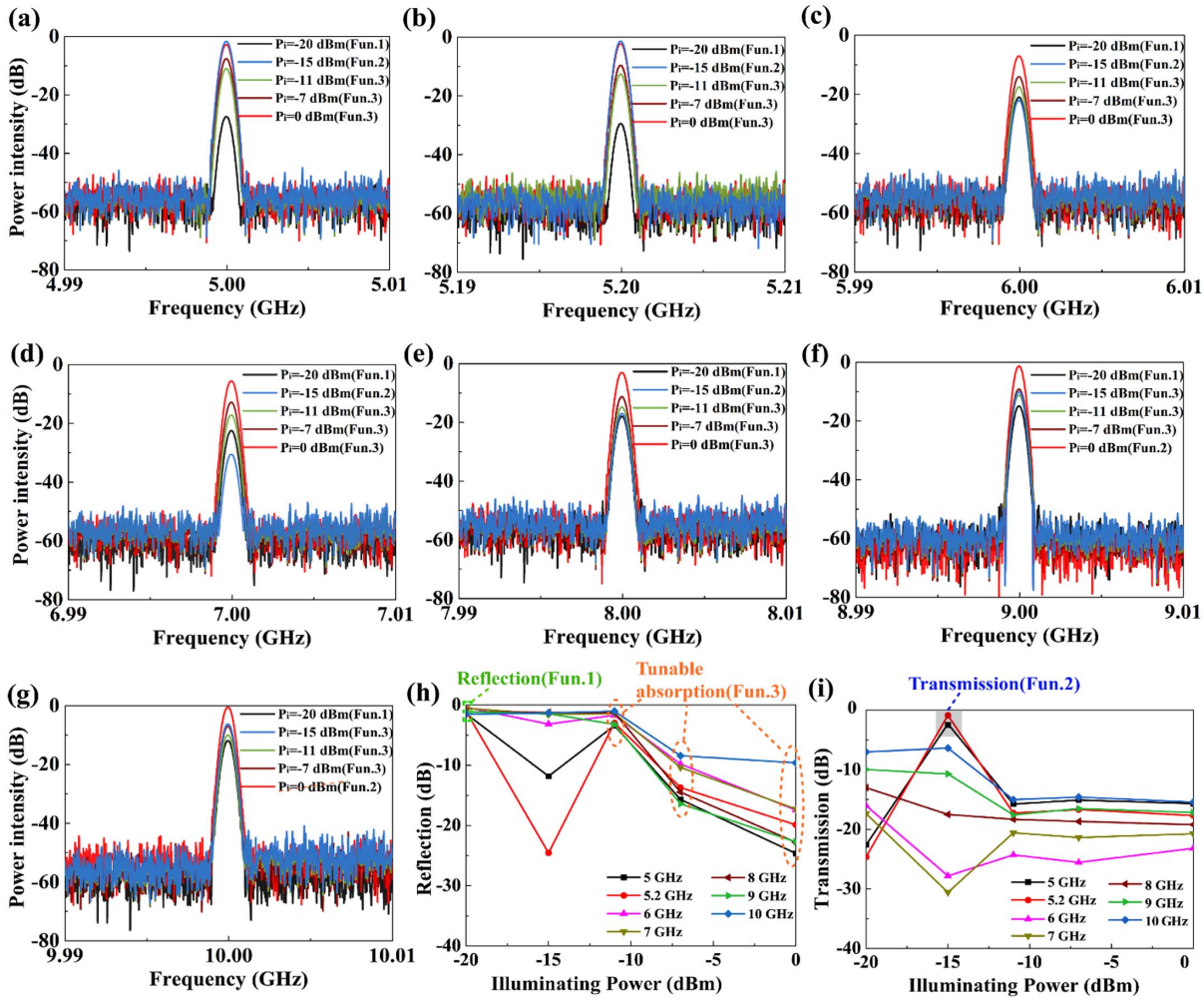

Fig. 6. (a)–(g) Transmitted power intensity of the metasurface under the different incident power intensities at the frequency of 5, 5.2, 6, 7, 8, 9, and 10 GHz. (h), (i) Measured reflection and transmission of the proposed metasurface for the different illuminating power intensities.

T-horn (R-horn 1/2) and the sample is about 1.0 m. Here, the VNA was set as "CW mode," which can achieve the signal output of a single frequency point. A DC power source (ITECH IT6322) was used to provide the constant offset voltage for the sample and FPGA platform. For the transmission measurement, the setup was normalized without a sample, and the illumination power is fixed as −15 dBm at the different frequency points. For the reflection measurement, a metallic plate with an identical dimension was used as a reference to standardize the reflection coefficient.

Funding. National Natural Science Foundation of China (61975209); Strategic High-technology Innovation Fund of the Chinese Academy of Sciences (CXJJ-19-B09); Sichuan Science and Technology Program (2020JDJQ0006); Sichuan Science and Technology Program (2020YFJ0001); Frontier Research Fund of Institute of Optics and Electronics, Chinese Academy of Sciences (C21K001).

Disclosures. The authors declare no conflicts of interest.

Data Availability. Data underlying the results presented in this paper are not publicly available at this time but may be obtained from the authors upon reasonable request.

REFERENCES

1. M. A. McEvoy and N. Correll, "Materials that couple sensing, actuation, computation, and communication," Science **347**, 1261689 (2015).
2. C. Kaspar, B. Ravoo, W. van der Wiel, S. Wegner, and W. Pernice, "The rise of intelligent matter," Nature **594**, 345–355 (2021).
3. O. Tsilipakos, A. C. Tasolamprou, A. Pitilakis, F. Liu, X. Wang, M. S. Mirmoosa, D. C. Tzarouchis, S. Abadal, H. Taghvaee, and C. Liaskos, "Toward intelligent metasurfaces: the progress from globally tunable metasurfaces to software-defined metasurfaces with an embedded network of controllers," Adv. Opt. Mater. **8**, 2000783 (2020).
4. T. Cui, B. Bai, and H. Sun, "Tunable metasurfaces based on active materials," Adv. Funct. Mater. **29**, 1806692 (2019).
5. A. Nemati, W. Qian, M. Hong, and J. Teng, "Tunable and reconfigurable metasurfaces and metadevices," Opto-Electron. Adv. **1**, 18000901 (2019).
6. C. Huang, J. Yang, X. Wu, J. Song, M. Pu, C. Wang, and X. Luo, "Reconfigurable metasurface cloak for dynamical electromagnetic illusions," ACS Photon. **5**, 1718–1725 (2017).

7. C. Huang, B. Zhao, J. Song, C. Guan, and X. Luo, "Active transmission/absorption frequency selective surface with dynamical modulation of amplitude," IEEE Trans. Antennas Propag. **69**, 3593–3598 (2021).
8. K. Chen, Y. Feng, F. Monticone, J. Zhao, B. Zhu, T. Jiang, L. Zhang, Y. Kim, X. Ding, and S. Zhang, "A reconfigurable active Huygens' metalens," Adv. Mater. **29**, 1606422 (2017).
9. M. Rahmani, L. Xu, A. E. Miroshnichenko, A. Komar, R. Camacho-Morales, H. Chen, Y. Zárate, S. Kruk, G. Zhang, and D. N. Neshev, "Reversible thermal tuning of all-dielectric metasurfaces," Adv. Funct. Mater. **27**, 1700580 (2017).
10. A. de Lustrac, B. Ratni, G. P. Piau, Y. Duval, and S. N. Burokur, "Tristate metasurface-based electromagnetic screen with switchable reflection, transmission, and absorption functionalities," ACS Appl. Electron. Mater. **3**, 1184–1190 (2021).
11. M. R. Shcherbakov, S. Liu, V. V. Zubyuk, A. Vaskin, P. P. Vabishchevich, G. Keeler, T. Pertsch, T. V. Dolgova, I. Staude, and I. Brener, "Ultrafast all-optical tuning of direct-gap semiconductor metasurfaces," Nat. Commun. **8**, 17 (2017).
12. H. S. Ee and R. Agarwal, "Tunable metasurface and flat optical zoom lens on a stretchable substrate," Nano Lett. **16**, 2818–2823 (2016).
13. E. Arbabi, A. Arbabi, S. M. Kamali, Y. Horie, M. S. Faraji-Dana, and A. Faraon, "MEMS-tunable dielectric metasurface lens," Nat. Commun. **9**, 812 (2018).
14. S. H. Badri, M. M. Gilarlue, S. SaeidNahaei, and J. S. Kim, "Narrowband-to-broadband switchable and polarization-intensitive terahertz metasurface absorber enabled by phase change material," J. Opt. **24**, 025101 (2021).
15. S. H. Badri, M. M. Gilarlue, S. G. Farkoush, and S. B. Rhee, "Reconfigurable bandpass optical filters based on subwavelength grating waveguides with $Ge_2Sb_2Te_5$ cavity," J. Opt. Soc. Am. B **38**, 1283–1289 (2021).
16. C. Huang, J. Yang, C. Ji, L. Yuan, and X. Luo, "Graphene-driven metadevice for active microwave camouflage with high-efficiency transmission window," Small Methods **5**, 2000918 (2021).
17. H. Wang, C. Hao, H. Lin, Y. Wang, L. Lan, C. Qiu, and H. Bao, "Generation of super-resolved optical needle and multifocal array using graphene oxide metalenses," Opto-Electron. Adv. **4**, 20003101 (2021).
18. B. Lee, J. Park, G. H. Han, H. Ee, C. Naylor, W. Liu, A. T. Charlie, and J. Agarwal, "Fano resonance and spectrally modified photoluminescence enhancement in monolayer MoS_2 integrated with plasmonic nanoantenna array," Nano Lett. **15**, 3646–3653 (2015).
19. R. Kowerdziej, M. Olifierczuk, J. Parka, and J. Wrobel, "Terahertz characterization of tunable metamaterial based on electrically controlled nematic liquid crystal," Appl. Phys. Lett. **105**, 022908 (2014).
20. C. Huang, J. Song, C. Ji, J. Yang, and X. Luo, "Simultaneous control of absorbing frequency and amplitude using graphene capacitor and Active frequency-selective surface," IEEE Trans. Antennas Propag. **69**, 1793–1798 (2021).
21. R. Wu, L. Bao, L. Wu, and T. J. Cui, "Broadband transmission-type 1-bit coding metasurfaces for electromagnetic beam forming and scanning," Sci. China Phys. Mech. Astron. **63**, 284211 (2020).
22. T. J. Cui, M. Qi, X. Wan, J. Zhao, and Q. Cheng, "Coding metamaterials, digital metamaterials and programming metamaterials," Light Sci. Appl. **3**, e218 (2014).
23. C. Huang, B. Sun, W. Pan, J. Cui, X. Wu, and X. Luo, "Dynamical beam manipulation based on 2-bit digitally-controlled coding metasurface," Sci. Rep. **7**, 42302 (2017).
24. L. Zhang, Z. X. Wang, R. W. Shao, J. L. Shen, X. Q. Chen, X. Wan, Q. Cheng, and T. J. Cui, "Dynamically realizing arbitrary multi-bit programmable phases using a 2-bit time-domain coding metasurface," IEEE Trans. Antennas Propag. **68**, 2984–2992 (2020).
25. Q. Ma and T. J. Cui, "Information metamaterials: bridging the physical world and digital world," PhotoniX **1**, 1 (2020).
26. J. Liao, S. Guo, L. Yuan, C. Ji, C. Huang, and X. Luo, "Independent manipulation of reflection amplitude and phase by a single-layer reconfigurable metasurface," Adv. Opt. Mater. 2101551 (2021).
27. R. Feng, B. Ratni, J. Yi, H. Zhang, A. de Lustrac, and S. N. Burokur, "Versatile metasurface platform for electromagnetic wave tailoring," Photon. Res. **9**, 1650–1659 (2021).
28. B. Liu, Y. He, S. W. Wong, and Y. Li, "Multifunctional vortex beam generation by a dynamic reflective metasurface," Adv. Opt. Mater. **9**, 2001689 (2021).
29. H. L. Wang, H. F. Ma, M. Chen, S. Sun, and T. J. Cui, "A reconfigurable multifunctional metasurface for full-space controls of electromagnetic waves," Adv. Funct. Mater. **31**, 2100275 (2021).
30. C. Huang, C. Ji, B. Zhao, J. Peng, L. Yuan, and X. Luo, "Multifunctional and tunable radar absorber based on graphene-integrated active metasurface," Adv. Mater. Technol. **6**, 2001050 (2021).
31. C. Huang, C. Zhang, J. Yang, B. Sun, B. Zhao, and X. Luo, "Reconfigurable metasurface for multifunctional control of electromagnetic waves," Adv. Opt. Mater. **5**, 1700485 (2017).
32. R. Phon, S. Ghosh, and S. Lim, "Novel multifunctional reconfigurable active frequency selective surface," IEEE Trans. Antennas Propag. **67**, 1709–1718 (2018).
33. Q. Ma, G. D. Bai, H. B. Jing, C. Yang, L. Li, and T. J. Cui, "Smart metasurface with self-adaptively reprogrammable functions," Light Sci. Appl. **8**, 98 (2019).
34. Q. Ma, Q. R. Hong, X. X. Gao, H. B. Jing, C. Liu, G. D. Bai, Q. Cheng, and T. J. Cui, "Smart metasurface with self-adaptively reprogrammable functions," Nanophotonics **9**, 3271–3278 (2020).
35. C. Qian, B. Zheng, Y. Shen, L. Jing, E. Li, L. Shen, and H. Chen, "Deep-learning-enabled self-adaptive microwave cloak without human intervention," Nat. Photonics **14**, 383–390 (2020).
36. H. Li, Q. Cao, L. Liu, and Y. Wang, "An improved multifunctional active frequency selective surface," IEEE Trans. Antennas Propag. **66**, 1854–1862 (2018).